dosimetry following intraperitoneal rhenium-186-labeled monoclonal antibody. *J Nucl Med* 1995;36:754–761.
15. Vriesendorp HM, Quadri SM, Andersson BS, et al. Hematologic side effects of radiolabeled immunoglobulin therapy. *Exp Hematol* 1996;24:1183–1190.
16. Finkler NJ, Muto MG, Kassis AI, et al. Intraperitoneal radiolabeled OC 125 in patients with advanced ovarian cancer. *Gynecol Oncol* 1989;34:339–344.
17. De Jager R, Abdel-Nabi H, Serafini A, et al. Current status of cancer immunodetection with radiolabeled human monoclonal antibodies. *Semin Nucl Med* 1993;23:165–179.
18. Griffin TW, Collins J, Bokhari F, et al. Intraperitoneal immunoconjugates. *Cancer Res* 1990;50(suppl):1031s–1038s.
19. Horan Hand P, Shrivastav S, Colcher D, et al. Pharmacokinetics of radiolabeled monoclonal antibodies following intraperitoneal and intravenous administration in rodents, monkeys and humans. *Antibody Immunoconj Radiopharm* 1989;2:241–255.
20. Leichner PK, Yang N-C, Frenkel TL, et al. Dosimetry and treatment planning for ^{90}Y-labeled antiferritin in hepatoma. *Int J Radiat Oncol Biol Phys* 1988;14:1033–1042.
21. Vriesendorp HM, Quadri SM, Williams JP. Radioimmunotherapy. In: Armitage JO, Antman K, eds. *High dose cancer therapy*. Philadelphia: Williams and Wilkins; 1992:84–123.
22. Freedman RS, Ioannides CG, Tomasovic B, et al. Development of a cell surface reacting human monoclonal antibody recognizing ovarian and certain other malignancies. *Hybridoma* 1991;10:21–33.
23. Chen P-F, Freedman RS, Chernajovsky Y, et al. Amplification of immunoglobulin transcripts by the non-palindromic adaptor polymerase chain reaction (NPA-PCR). Nucleotide sequence analysis of two human monoclonal antibodies recognizing two cell surface antigens expressed in ovarian, cervix, breast, colon and other carcinomas. *Hum Antibodies Hybridomas* 1994;5:131–142.
24. Quadri SM, Mohammadpour H. Synthesis of 2-*p*-aminobenzyl-3-methyl-and 2-*p*-aminobenzyl-3-benzyl derivatives of diethyleneaminepentaacetic acids (DTPA): carbon backbone modified bifunctional chelating agents. *Bioorg Med Chem Lett* 1992;2:1661–1664.
25. Quadri SM, Vriesendorp HM, Leichner PK, et al. Evaluation of indium-111- and yttrium-90-labeled linker-immunoconjugates in nude mice and dogs. *J Nucl Med* 1993;34:938–945.
26. Mujoo K, Maneval DC, Anderson SC, et al. Adenoviral-mediated p53 tumor suppressor gene therapy of human ovarian carcinoma. *Oncogene* 1996;12:1617–1623.
27. Quadri SM, Malik AB, Tang XZ, et al. Preclinical analysis of intraperitoneal administration of ^{111}In-labeled human tumor reactive monoclonal IgM AC6C3–2B12. *Cancer Res* 1995;55(suppl):5736s–5742s.
28. Quadri SM, Malik AB, Chu HB, et al. Intraperitoneal indium-111 and yttrium-90-labeled human IgM (AC6C3–2B12) in nude mice bearing peritoneal carcinomatosis. *J Nucl Med* 1996;37:1545–1551.
29. Wahl RL, Barrett J, Geatti O, et al. The intraperitoneal delivery of radiolabeled monoclonal antibodies: studies on the regional delivery advantage. *Cancer Immunol Immunother* 1988;26:187–201.
30. Jullien-Vitoux D, Voisin GA. Studies in vascular permeability II. Comparative extravasation of different immunoglobulin classes in normal pig skin. *Eur J Immunol* 1973;3:663–667.
31. Halpern SE, Hagan PL, Chen A, et al. Distribution of radiolabeled human and mouse monoclonal IgM antibodies in murine models. *J Nucl Med* 1988;29:1688–1696.
32. Quadri SM, Shao Y, Blum JE, et al. Preclinical evaluation of intravenously administered ^{111}In- and ^{90}Y-labeled B72.3 immunoconjugate (GYK-DTPA) in beagle dogs. *Nucl Med Biol* 1993;20:559–570.
33. Wang S, Quadri SM, Tang X-Z, et al. Liver toxicity induced by combined external beam irradiation and radioimmunoglobulin therapy. *Radiat Res* 1995;141:292–302.
34. Hird V, Maraveyas A, Snook D, et al. Adjuvant therapy of ovarian cancer with radioactive monoclonal antibody. *Br J Cancer* 1993;68:403–406.

Pharmacokinetic Model of Iodine-131-G250 Antibody in Renal Cell Carcinoma Patients

Angela Loh, George Sgouros, Joseph A. O'Donoghue, Devie Deland, Dennis Puri, Peter Capitelli, John L. Humm, Steven M. Larson, Lloyd J. Old and Chaitanya R. Divgi

Department of Medical Physics and Department of Radiology, Nuclear Medicine Service, Memorial Sloan-Kettering Cancer Center; and Ludwig Institute for Cancer Research, New York, New York

A model that describes the pharmacokinetic distribution of ^{131}I-labeled G250 antibody is developed. **Methods:** Previously collected pharmacokinetic data from a Phase I–II study of ^{131}I-G250 murine antibody against renal cell carcinoma were used to develop a mathematical model describing antibody clearance from serum and the whole body. Survey meter measurements, obtained while the patient was under radiation precautions, and imaging data, obtained at later times, were combined to evaluate whole-body clearance kinetics over an extended period. **Results:** A linear two-compartment model was found to provide good fits to the data. The antibody was injected into Compartment 1, the initial distribution volume (V_d) of the antibody, which included serum. The antibody exchanged with the rest of the body, Compartment 2, and was eventually excreted. Data from 13 of the 16 patients fit the model with unique parameters; the maximum, median and minimum values for model-derived V_d were 6.3, 3.7 and 2.11, respectively. The maximum, median and minimum values for the excretion rate were 8×10^{-2}, 2.4×10^{-2} and 1.3×10^{-2} hr^{-1}, respectively. Parameter sensitivity analysis showed that a change in the transfer rate constant from serum to the rest of the body had the greatest effect on serum cumulative activity and that the rate constant for excretion had the greatest effect on whole-body cumulative activity. **Conclusion:** A linear two-compartment model was adequate in describing the serum and whole-body kinetics of G250 antibody distribution. The median initial distribution volume predicted by the model was consistent with the nominal value of 3.81. A wide variability in fitted parameters was observed among patients, reflecting the differences in individual patient clearance and exchange kinetics of G250 antibody. By selecting median parameter values, such a model may be used to evaluate and design prolonged multiple administration radioimmunotherapy protocols.

Key Words: radioimmunotherapy; modeling; antibody; treatment planning; pharmacokinetics

J Nucl Med 1998; 39:484–489

With the advent of humanized antibodies and the accompanying reduction in immunogenicity, fractionated dosing of antibodies over protracted time periods will be feasible. Because of the increased complexity of such trials, pharmacokinetic modeling will be important in evaluating administration protocols and their potential efficacy and toxicity. Studies of radioimmunotherapy in mice have shown that greater doses can be tolerated, and toxicity reduced, with fractionated administration (*1,2*). Patient studies also have suggested that this is the case but have been limited by the induction of an immune response against murine-derived antibody (*3–5*). Little is known about the potential marrow-sparing effects of prolonged, multiple-administration radioimmunotherapy or how best to design prolonged fractionated treatment protocols. Modeling will allow evaluation of various dosing schedules according to quantifiable criteria, such as predicted clearance rates, residence times and absorbed doses. Information obtained from single-administration protocols may be used to establish mathematical models of radiolabeled antibody distribution and dosimetry. Such models may then be used to simulate prolonged, multiple-

Received Dec. 23, 1996; revision accepted May 6, 1997.
For correspondence or reprints contact: George Sgouros, PhD, Department of Medical Physics, Memorial Sloan-Kettering Cancer Center, New York, NY 10021.

administration protocols and from such simulations derive quantifiable criteria. This approach to treatment design may be particularly important in devising outpatient protocols, wherein the retained activity must not exceed a specified regulatory limit.

A wide variety of mathematical models has been developed to evaluate different approaches to radioimmunotherapy. Modeling has been used to: evaluate the use of unlabeled (cold) antibody to saturate antigen sites in liver or spleen and thereby improve radioimmunodiagnosis or radioimmunotherapy (*6,7*); examine the differences between intact antibody and antibody fragments with regard to distribution, catabolism and excretion (*8*); understand the effect of circulating antigen on antibody distribution (*9*); optimize two-step approaches (using bifunctional antibodies and haptens) (*10–12*); optimize administered amounts (*13–15*); and simulate plasmapheresis or extracorporeal immunoadsorption for improving therapy or diagnosis by clearing the plasma of excess unbound antibody (*16–18*). We developed a mathematical model that describes the pharmacokinetic distribution of ^{131}I-labeled G250 antibody against renal cell carcinoma (*19*).

MATERIALS AND METHODS

Patients

Sixteen patients (4 women, 12 men; age range 40–79 yr) with renal cell carcinoma participating in a Phase I–II activity-escalation study of ^{131}I-labeled G250 antibody were used. Their weights ranged from 60 to 107 kg, and their heights ranged from 158 to 188 cm. Patients at each dose level were given one injection of antibody each, with different levels of activity. Those at the first dose level were administered 10 mg G250 antibody with 30 mCi/m^2 ^{131}I. Those at subsequent levels received higher levels of activity in 15 mCi/m^2 increments, also administered on 10 mg antibody, until the highest dose level of 90 mCi/m^2 was reached. After injection, survey meter measurements, blood samples and planar images were taken.

Whole-Body Kinetics

A whole-body clearance curve for each patient was obtained by combining survey meter measurements, taken during patient isolation, with imaging data, collected after release from isolation. Because patients at higher dose levels could not be imaged due to radiation safety constraints, we generally took survey meter measurements immediately after injection and every day thereafter until the patients could be released from hospital isolation. These measurements were recorded using a handheld ionization chamber (Keithley Radiation Survey Meter, Keithley Inc., Cleveland, OH). All measurements were made 1 m away from the patient's sternum. The measurements were decay corrected and converted to the percentage of injected dose.

Whole-body images were obtained using ADAC (Milpitas, CA) dual-headed Genesys cameras with high-energy, general purpose collimation. Whole-body activity was obtained from the geometric mean of anterior and posterior counts. Contours were drawn around the whole body and a background region. Background-corrected results were expressed as counts per pixel per second. A calibration standard was kept in the field of view for all images. This was used to correct for variations in camera sensitivity over the imaging interval for each patient. Patient thickness, obtained from each patient's CT scan was used for attenuation correction, with an attenuation coefficient of 0.1 cm^{-1} (*20*). A composite, whole-body clearance curve was produced by combining the imaging data, expressed as the percentage of the injected activity, with the survey meter measurements. Because imaging data points usually began after the last survey meter measurement, we fit an exponential curve to the survey meter measurements. This exponential expression was then used to place the first imaging data point along the curve. All subsequent imaging data points were scaled using the scaling factor used for the first point. If imaging and survey meter measurements overlapped in time, we used survey meter measurements.

Serum Clearance

Throughout the course of treatment, blood samples were drawn and activity in the serum was counted in an LKB Wallac gamma counter (Gaithersburg, MD) and expressed as the percentage of the injected dose per liter.

Model Design

The two-compartment model describing antibody clearance from blood and the whole body is shown in Figure 1. Compartment 1 represents the initial distribution volume of the antibody (e.g., plasma and ECF of red marrow, liver and spleen). Compartment 2 represents the remainder of the body. Excretion occurs from Compartment 2. The equations governing this model are provided in the appendix. The Simulation Analysis and Modeling Package (SAAM II) developed at the Resource Facility for Kinetic Analysis (*21,22*) was used for fitting. Serum activity concentration data were assigned to Compartment 1. Whole-body clearance data were assigned to the sum of Compartments 1 and 2. The serum activity concentration was multiplied by the distribution volume as shown in the appendix. All pharmacokinetic data were decay corrected. The data were weighted for fitting assuming Poisson statistics. Fits were obtained by varying the three exchange rate constants, k (2,1), k (1,2), k (0,2) and the initial distribution volume, V_d.

Distribution Volume Comparison

Patients with model-derived V_ds that were 2 s.d.s outside the expected mean value were identified using the plasma volume (V_p) equation of the International Commission on Radiological Protection (*23*):

$$V_p = W \cdot 45.02e^{-0.0014 \cdot Y}. \quad \text{Eq. 1}$$

Given the patient's weight (W in kg) and age (Y in years), Equation 1 provides an estimate of plasma volume in milliliters. The standard deviation associated with the volume estimate was 6.75 ml/kg body weight (*23*).

Assuming that the extracellular fluid volume of spleen, liver and red marrow was 0.81 for a standard V_p of 3.01 (*23*), the nominal standard V_d is 3.81 (*14*). Patient-specific V_ds were obtained by scaling V_p:

$$V_d = V_p \cdot \frac{3.8}{3.0}. \quad \text{Eq. 2}$$

The data for patients whose model-derived V_d was 2 s.d.s outside the value given by Equation 2 were examined in more detail to determine whether the unusually large or small V_d could be explained by known pathology or physiology.

Parameter Sensitivity Analysis

The median value for each parameter was chosen to represent a set of standard parameters for the G250 model. The degree and time course of each parameter's sensitivity was assessed by performing model simulations in which one parameter was varied and all others were kept fixed. Simulated curves were generated to determine the effect of each parameter on serum and whole-body clearance and the time during which these were most sensitive to parameter variations. The kinetic curves obtained for each simulation were integrated over time to indicate the effect of each parameter on the area under the curve (AUC) for serum and total body. Parameter V_d was not varied because it is a linear conversion

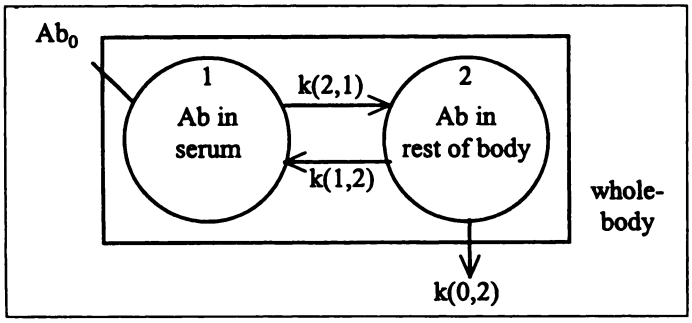

FIGURE 1. Pharmacokinetic model used to fit patient data. The parameters, k (2,1) and k (1,2) are the vascular-to-extravascular antibody transfer rate constants. Initially, an amount of antibody, Ab_0, is injected intravenously (Compartment 1). The excretion rate is k (0,2).

factor from activity concentration to activity (see Eq. 3 in the Appendix).

RESULTS

Parameter fits were obtained for 13 of the 16 patients considered. Figure 2, Panels 1–16, illustrate the patient data with model-derived, fitted curves. The parameters obtained for each patient are listed in Table 1. The data from Patients 14, 15 and 16 did not yield a unique set of parameter values; the values shown in the table were used to generate Panels 14–16 in Figure 2. They are one of a large number of parameter sets that could fit the data. The standard deviations in parameter values listed for other patients reflect the reliability of individual parameter estimates.

Patients whose parameters had particularly large standard deviations had data points that could be considered outliers. For example, the fractional standard deviation of parameter k (1,2) for Patient 10 was 3.3. The second survey meter measurement for this patient exceeded the 100% injected dose level.

The V_ds predicted by the model ranged from 2 to 6.3 liters, with a median of 3.71. Patients 5 and 9 had model-derived V_ds that were greater than 2 s.d.s above a weight- and age-adjusted population mean (*23*). An exceptionally high model-derived V_d can be explained by loss of antibody from circulation due to an increase in binding. For instance, patients with larger tumors and, therefore, an increased number of antigen sites or patients whose antigen sites are more accessible will have a lower concentration of antibody in circulation due to antigen binding. Increased antigen expression in cross-reactive organs, such as large bile ducts in the case of G250, or increased accessibility to these sites also will produce higher model-derived estimates of V_d.

Patient 9 presented with the largest tumor burden, 12.5 kg, as measured by CT. Patient 5, however, had a relatively small tumor at 54 g, suggesting that other factors might be causing the high V_d value. Except for Patient 15, who had a tumor mass of 1.3 kg, all other patients had tumor masses below 1.0 kg. The distribution volume obtained for Patient 15 also was 2 s.d.s greater than a weight- and age-adjusted mean. The estimate, however, was obtained from a nonunique fit to the data.

Model-derived estimates of V_d for Patients 4, 6, 7 and 8 were below 2 s.d.s from the expected mean value. Data from these patients were more difficult to explain because the factors mentioned earlier only explained high V_d values. Low values can be caused by a reduction in vascular space, such as nephrectomy, splenectomy or reduced liver function. Antigen-negative, space-occupying disease also can explain low V_d values. Although more than 75% of clear cell renal carcinoma expresses G250 antigen, there is still a degree of variability so that some sites of disease show no expression and other sites exhibit 100% expression (*19*). An upper limit on this as a potential explanation for the low V_d values may be obtained by assuming that all of these patients' disease is antigen negative and occupies what would otherwise be distribution space. The corrected distribution volumes for Patients 4 and 7 were within the 2-s.d. range if these assumptions are made. Patients 6 and 8, however, still had model-derived V_d values that were lower than expected.

The curves obtained in the parameter variation study are depicted in Figures 3A–3F. At early times after injection, serum kinetics have the greatest impact on k (2,1) and a minimal influence on k (0,2) (Figs. 3A and 3C). This is consistent with the structure of the model; k (2,1) is the transfer rate from serum to the rest of the body. This term, and the rate of return, k (1,2), dominates the kinetics until serum and rest-of-body equilibrate. Once an equilibrium between serum and the rest of the body is reached, the clearance rate for both curves is determined by k (0,2), the excretion rate. Because excretion is represented by a direct clearance from the rest-of-body compartment, k (0,2) has the greatest impact on the whole-body curve throughout the simulation time (Fig. 3F). Table 2 shows the percentage of change in the AUC for serum and total body, when the median parameters are increased or reduced by a factor of 2. As expected, from the discussion earlier, k (2,1) and k (1,2) have a greater impact on serum rather than on whole-body AUC, whereas the opposite is true for k (0,2). The parameter k (2,1) has the greatest impact on serum AUC. This parameter influences serum kinetics when the serum curve is at its highest level. Changes during this period will, therefore, have the greatest impact on the overall AUC.

CONCLUSION

Several other investigators have developed pharmacokinetic models of antibody distribution. Zanzonico et al. (*24*) developed a multicompartmental model for an ^{131}I-labeled anticarcinoembryonic antigen antibody. The model specifically incorporated the effects of radionuclide dissociation and free iodide metabolism and excretion. The remainder-of-body compartment in this model was resolved into rapidly and slowly exchanging tissues, as initially defined by Dewey (*25*). Transfer rates from the vascular to extravascular (or remainder-of-body) compartment were set to 0.07 hr^{-1} and 0.02 hr^{-1} for rapidly and slowly exchanging tissues, respectively. The return rates were correspondingly set to 0.05 and 0.014 hr^{-1}. Median values obtained for the corresponding G250 antibody exchange rates, k (2,1) and k (1,2), were 0.043 and 0.020 hr^{-1}. These values lie between the rapidly and slowly exchanging tissue values used by Zanzonico et al. (*24*). Rate constants for rapidly exchanging tissue were used by Koizumi et al. (*6*) in a model of ^{131}I-Lym-1 (anti-B cell lymphoma) antibody. The model included a nonlinear term that was primarily associated with liver processing of the antibody (*6*). In a model of ^{111}In-9.2.27, antimelanoma, antibody distribution, data from 12 patients were used to estimate vascular to extravascular exchange rates (*7*). Mean values of 0.1 and 0.3 hr^{-1} for parameters corresponding to k (2,1) and k (1,2), respectively, were obtained. The high 0.3 hr^{-1} return rate obtained in the study was noted to be inconsistent with expected values but could not be explained. In this study, individual estimates of k (2,1) and k (1,2) with fractional standard deviations less than 1 ranged from 0.021 to 0.09 and 0.005 to 0.14, respectively. The ratio, k (2,1)/k (1,2), which is equal to the ratio of the extravascular-to-vascular antibody V_d at equilibrium, ranged from 0.5 to 8, with a median of 1.5. The median value is consistent with the value of 1.4 reported in animal studies (*25*).

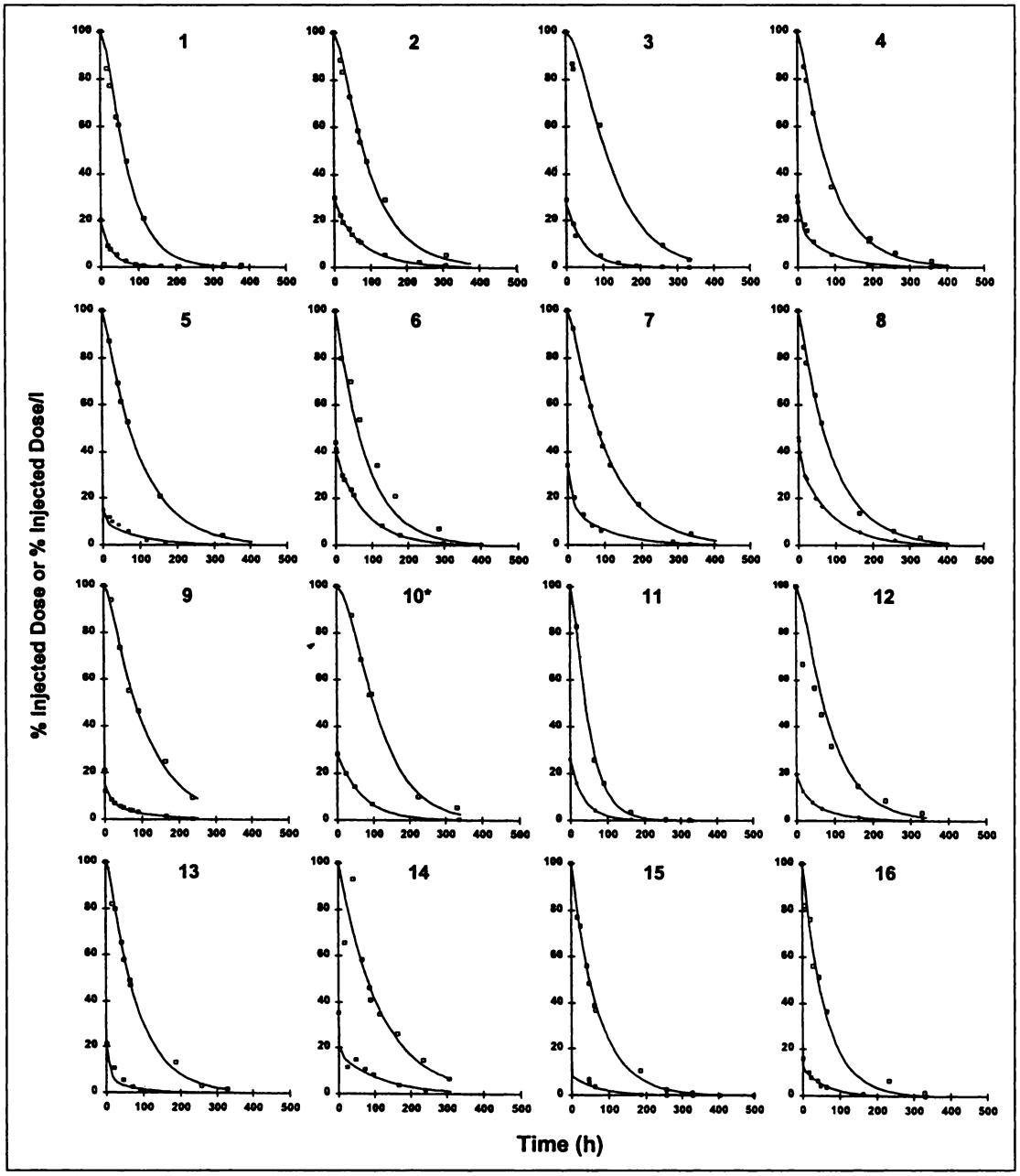

FIGURE 2. Whole-body activity (open squares) and serum activity concentration (solid squares) in the percentage of injected dose and the percentage of injected dose per liter, respectively. Model fits for both sets of data are shown by the solid lines. Note, the second whole-body data point, which exceeded 100% of injected dose, is not plotted for this patient.

In this article, we present a two-compartment pharmacokinetic model that describes the distribution of an antibody in serum and in the whole body. In almost all patients considered, the model provided adequate and unique fits to the data. This was indicated by the standard deviations of the parameter estimates and the consistency with which the model was able to fit data from several different patients to yield parameters that were consistent with values in the literature. It was possible to fit these data without invoking a nonlinear component suggesting minimal cross-reactivity or processing by liver or other tissues. Although the two-compartment model is a simplification, measurements in individual tissues and in tumor would be needed to resolve additional compartments and to introduce nonlinear components.

Pharmacokinetic modeling of radiolabeled antibody has made it possible to combine measured patient data with data obtained from animal studies or from studies in vitro (*26*). As new, nonimmunogenic antibody constructs are generated (*27,28*), prolonged multiple-administration treatment may become possible. It will not be feasible to investigate clinically all the various treatment and dosing options that will become available with multiple dosing. Data from initial, single-administration protocols can be used to develop pharmacokinetic models that may then be used to simulate multiple-administration treatment regimens. Such modeling will help reduce the range of possible treatment schedules that merit clinical investigation.

ACKNOWLEDGMENTS

This work was supported partly by National Institutes of Health Grants R01 CA62444 and P01 CA33049. Devie Deland and Dennis Puri are recipients of the Frank J. Scallon Medical Science Award.

TABLE 1
Fitted Parameter Values (± s.d.)

Patient no.	Parameters			
	k (2,1) (hr^{-1})	k (1,2) (hr^{-1})	k (0,2) (hr^{-1})	V_d (liters)
1	0.040 ± 0.002	0.005 ± 0.001	0.022 ± 0.001	5.0 ± 0.2
2	0.022 ± 0.004	0.018 ± 0.006	0.030 ± 0.004	3.3 ± 0.2
3	0.021 ± 0.002	0.0003 ± 0.0006	0.013 ± 0.001	3.7 ± 0.2
4	0.06 ± 0.02	0.05 ± 0.02	0.024 ± 0.004	3.3 ± 0.3
5	0.07 ± 0.03	0.08 ± 0.03	0.025 ± 0.009	6.0 ± 1
6	0.06 ± 0.04	0.3 ± 0.3	0.08 ± 0.01	2.28 ± 0.05
7	0.053 ± 0.008	0.035 ± 0.007	0.018 ± 0.001	2.9 ± 0.2
8	0.07 ± 0.02	0.14 ± 0.06	0.040 ± 0.003	2.13 ± 0.04
9	0.043 ± 0.009	0.022 ± 0.008	0.017 ± 0.002	6.3 ± 0.5
10	0.0146 ± 0.0003	0.0001 ± 0.0003	0.019 ± 0.001	3.54 ± 0.03
11	0.033 ± 0.003	0.012 ± 0.005	0.063 ± 0.005	3.79 ± 0.06
12	0.031 ± 0.002	0.017 ± 0.003	0.026 ± 0.002	5.03 ± 0.05
13	0.09 ± 0.03	0.020 ± 0.009	0.017 ± 0.001	4.2 ± 0.7
14*	0.47	0.44	0.02	2.84
15*	1.43	0.74	0.02	4.29
16*	0.91	0.52	0.03	3.22

*Standard deviations were not available because parameters were not unique.

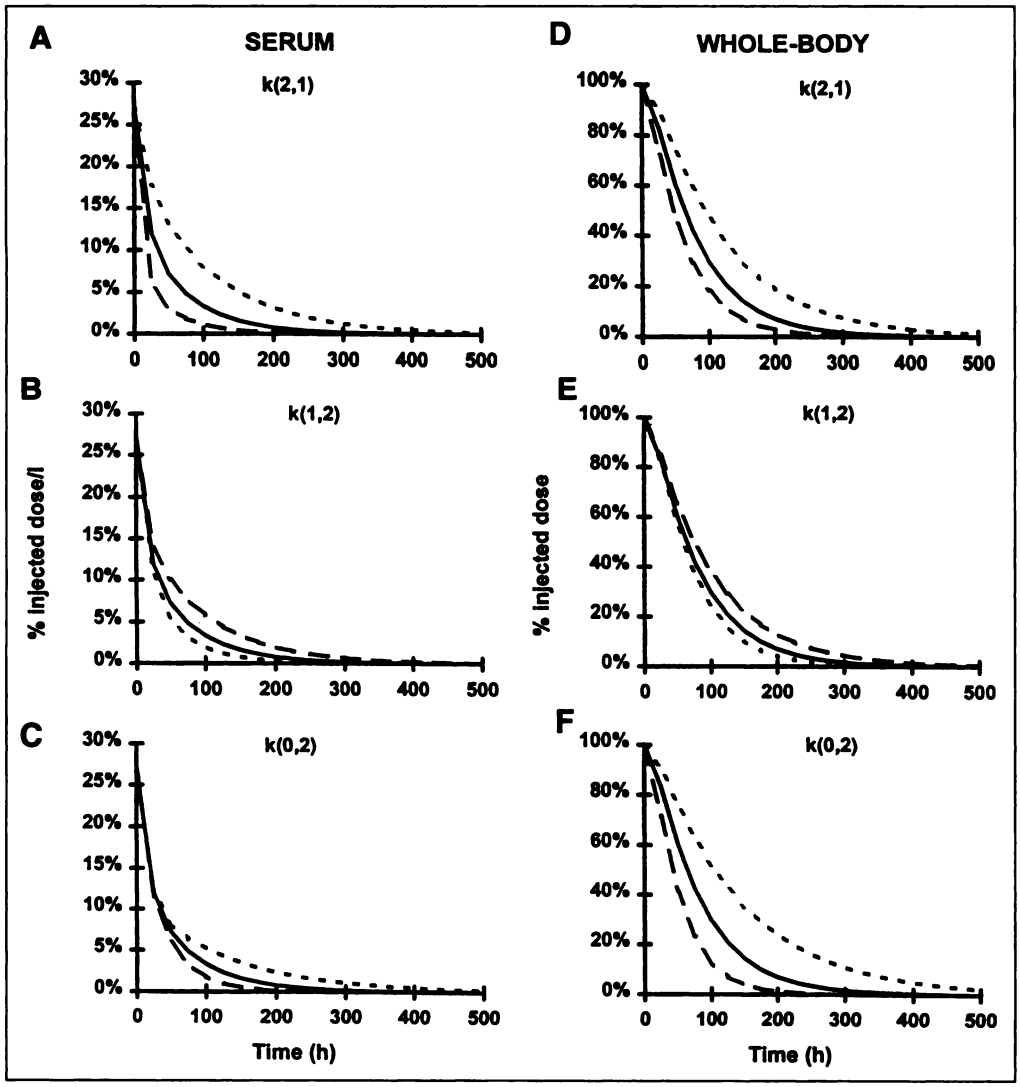

FIGURE 3. Sensitivity of serum and whole-body kinetics to parameter values. Simulated curves for median (solid line), median × 2 (dashed) and median ÷ 2 (dotted) parameter values are shown in each plot. The parameter that was varied is listed on the top of the plot.

TABLE 2
Model Sensitivity to Parameter Values

Parameter change*	% change in AUC		
	k (2,1)	k (1,2)	k (0,2)
Median × 2			
Serum	−50	45	−22
Total body	−25	23	−36
Median ÷ 2			
Serum	98	−22	43
Total body	50	−11	69

*Median values: k (2,1) = 0.043, k (1,2) = 0.020, k (0,2) = 0.024 (hr^{-1}).
AUC = area under the curve.

APPENDIX

$$\frac{dAb_1}{dt} = -k(2,1) \cdot Ab_1 + k(1,2) \cdot Ab_2 \quad \text{Eq. A1}$$

$$\frac{dAb_2}{dt} = k(2,1) \cdot Ab_1 - k(1,2) \cdot Ab_2 - k(0,2) \cdot Ab_2 \quad \text{Eq. A2}$$

$$Ab_1 = [Ab_1] \cdot V_d \quad \text{Eq. A3}$$

REFERENCES

1. Schlom J, Molinolo A, Simpson JF, et al. Advantage of dose fractionation in monoclonal antibody-targeted radioimmunotherapy. *J Natl Cancer Inst* 1990;82:763–771.
2. Buchsbaum D, Khazaeli MB, Liu T, et al. Fractionated radioimmunotherapy of human colon carcinoma xenografts with ^{131}I-labeled monoclonal antibody CC49. *Cancer Res* 1995;55(suppl):5881s–5887s.
3. DeNardo GL, DeNardo SJ, O'Grady LF, Levy NB, Adams GP, Mills SL. Fractionated radioimmunotherapy of B-cell malignancies with ^{131}I-Lym-1. *Cancer Res* 1990; 58(suppl):1014s–1016s.
4. Meredith RF, Khazaeli MB, Liu T, et al. Dose fractionation of radiolabeled antibodies in patients with metastatic colon cancer. *J Nucl Med* 1992;33:1648–1653.
5. Richman CM, DeNardo SJ, O'Grady LF, DeNardo GL. Radioimmunotherapy for breast cancer using escalating fractionated doses of ^{131}I-labeled chimeric L6 antibody with peripheral blood progenitor cell transfusions. *Cancer Res* 1995;55(suppl):5916s–5920s.
6. Koizumi K, DeNardo GL, DeNardo SJ, et al. Multicompartmental analysis of the kinetics of radioiodinated monoclonal antibody in patients with cancer. *J Nucl Med* 1986;27:1243–1254.
7. Eger RR, Covell DG, Carrasquillo JA, et al. Kinetic model for the biodistribution of an indium-111-labeled monoclonal antibody in humans. *Cancer Res* 1987;47:3328–3336.
8. Covell DG, Barbet J, Holton OD, Black CDV, Parker RJ, Weinstein JN. Pharmacokinetics of monoclonal immunoglobulin G_1, $F(ab')_2$, and Fab' in mice. *Cancer Res* 1986;46:3969–3978.
9. Rescigno A, Bushe H, Brill AB, Rusckowski M, Griffin TW, Hnatowich DJ. Pharmacokinetic modeling of radiolabeled antibody distribution in man. *Am J Physiol Imaging* 1990;5:141–150.
10. Yuan F, Baxter LT, Jain RK. Pharmacokinetic analysis of two-step approaches using bifunctional and enzyme-conjugated antibodies. *Cancer Res* 1991;51:3119–3130.
11. Baxter LT, Yuan F, Jain RK. Pharmacokinetic analysis of the perivascular distribution of bifunctional antibodies and haptens: comparison with experimental data. *Cancer Res* 1992;52:5838–5844.
12. van Osdol WW, Sung C, Dedrick RL, Weinstein JN. A distributed pharmacokinetic model of two-step imaging and treatment protocols: application to streptavidin-conjugated monoclonal antibodies and radiolabeled biotin. *J Nucl Med* 1993;34:1552–1564.
13. Mulshine JL, Shuke N, Daghighian F, et al. The correct dose: pharmacologically guided end point for anti-growth factor therapy. *Cancer Res* 1992;(suppl):2743s–2746s.
14. Sgouros G, Graham MC, Divgi CR, Larson SM, Scheinberg DA. Modeling and dosimetry of monoclonal antibody M195 (anti-CD33) in acute myelogenous leukemia. *J Nucl Med* 1993;34:422–430.
15. Sgouros G, Scheinberg DA. The treatment of leukemia with radiolabeled monoclonal antibodies. In: Rosen ST, Kuzel TM, eds. *Immunoconjuage therapy of hematologic malignancies*. Norwell, MA: Kluwer Academic; 1993:23–64.
16. Sgouros G. Plasmapheresis in radioimmunotherapy of micrometastases: a mathematical modeling and dosimetrical analysis. *J Nucl Med* 1992;33:2167–2179.
17. Hartmann C, Bloedow DC, Dienhart DG, et al. A pharmacokinetic model describing the removal of circulating radiolabeled antibody by extracorporeal immunoadsorption. *J Pharmacokin Biopharma* 1991;19:385–403.
18. Norrgren K, Strand S, Ingvar C. Contrast enhancement in RII and modification of the therapeutic ratio in RIT: a theoretical evaluation of simulated extracorporeal immunoadsorption. *Antibody Immunocon Radiopharm* 1992;5:61–73.
19. Oosterwijk E, Bander NH, Divgi CR, et al. Antibody localization in human renal cell carcinoma: a phase I study of monoclonal antibody G250. *J Clin Oncol* 1993;11:738–750.
20. Macey DJ, Grant EJ, Bayouth JE, et al. Improved conjugate view quantitation of iodine-131 by subtraction of scatter and septal penetration events with a triple energy window method. *Med Phys* 1995;22:1637–1643.
21. Berman M, Weiss MF. *SAAM manual* (DHEW Publication no. (NIH) 78-810). Washington, D.C.: U.S. Government Printing Office; 1978.
22. Foster DM, Boston RC, Jacquez JA, Zech LA. *The SAAM tutorials: an introduction to using conversational SAAM, version 30*. Seattle, WA: Resource Facility for Kinetic Analysis; 1989.
23. International Commission on Radiological Protection. *Report of the task group on reference man* (Publication no. 23). New York: Pergamon Press; 1975.
24. Zanzonico PB, Bigler RE, Primus FJ, et al. A compartmental modeling approach to the radiation dosimetry of radiolabeled antibody. In: Schlafke-Stelson AT, Watson EE, eds. In: *Proceedings of the Fourth International Dosimetry Symposium*. Oak Ridge, TN; 1985:421–445.
25. Dewey WC. Vascular-extravascular exchange of ^{131}I plasma proteins in the rat. *Am J Physiol* 1959;197:423–431.
26. Strand SE, Zanzonico P, Johnson TK. Pharmacokinetic modeling. *Med Phys* 1993;20: 497–611.
27. Caron PC, Jurcic JG, Scott AM, et al. A phase I B trial of humanized monoclonal antibody M195 (anti-CD33) in myeloid leukemia: specific targeting without immunogenicity. *Blood* 1994;83:1760–1768.
28. Yokota T, Milenic DE, Whitlow M, Schlom J. Rapid tumor penetration of a single-chain Fv and comparison with other immunoglobulin forms. *Cancer Res* 1992;52:3402–3408.

Erratum

There was an error in the concentration of SSKI in "Jod-Basedow Syndrome Following Oral Iodine and Radioiodinated-Antibody Administration" by El-Shirbiny et al. (*J Nucl Med* 1997;38:1816–1817). It should be 1 g/ml, not 1 mg/ml as published on page 1816, column 2, line 7 of the first full paragraph.